Electronic Supplementary Information

Non-integer induced spontaneous polarization of highly efficient perovskite-based NBTO SCNs photocatalyst

Yidong Hu,[a] Gang Chen,[*,a] Chunmei Li,[*b] Zhonghui Han,[a] Sue Hao,[a] Weizhao Hong[a] and Weinan Xing[a]

[a] School of Chemistry and Chemical Engineering, Harbin Institute of Technology, No. 92 West-Da Zhi Street, Harbin 150001 (China)

[b] Institute of Green Chemistry and Chemical Technology, School of Chemistry and Chemical Engineering, Jiangsu University, Zhenjiang 212013 (China)

[*]correspondence: gchen@hit.edu.cn, lichun_mei_happy@126.com

Experimental Procedures

Synthesis of $Na_{0.5}Bi_{2.5}Ta_2O_9$ nanoplates

All of the reagents were used as purchased without further purification. A typical synthesis of $Na_{0.5}Bi_{2.5}Ta_2O_9$ single-crystal nanoplates (NBTO SCNs), 2.5 mmol of Bi_2O_3, 2 mmol of Ta_2O_5 and 2.05 g eutectic salt (n_{NaCl}/n_{KCl} = 1) mixture vigorously grounded in agate mortar for 30 min. After that, the mixture was calcined in air at 750 °C for 24 h at ramp rate of 5 °C/min in tubular furnace using corundum porcelain boat. After cooling, pure NBTO SCNs was obtained after removing the salt flux with deionized water, and finally dried at 100 °C for 10 h. For comparison, $NaTaO_3$ and $BiTaO_4$ were synthesized by traditional solid-state reaction.[1, 2]

Characterization

Crystalline structures of the NBTO powders were characterized by powder X-ray diffraction (XRD, Rigaku D/max-2000, Cu/Kα1) monochromatized Cu-Kα radiation at scanning rate of 5˚ min^{-1} at room temperature. The morphologies were characterized by field-emission scanning electron microscopy (FESEM, FEI QUANTA 200F). Transmission electron microscopy (TEM) and high resolution TEM (HRTEM) were carried out on FEI Tecnai G2 S-Twin microscope at accelerating voltage of 300 kV. In order to check the binding energies of elements, X-ray photoelectron spectroscopy (XPS, Thermo ESCALAB 250Xi, a monochromatic Al Kα as the X-ray source) spectra were also carried out. The peak positions were calibrated using the C 1s peak at 284.8 eV of the surface extraneous carbon. UV-vis diffuse reflectance absorption spectrum (DRS) was obtained on Hitachi (UH4150) spectrophotometer with an integrating sphere attachment. The Na, Bi and Ta contents of the samples were determined using an inductively coupled plasma optical emission spectrometer (ICP-OES, Perkin Elmer Optima 5300DV, U.S.). The Brunauer-Emmett-Teller (BET) surface areas were obtained on Micromeritics ASAP 2020 adsorption analyzer under liquid nitrogen environment.

Photocatalytic activities

Photocatalytic hydrogen generation was conducted in a closed gas circulation system. A typical procedure, 0.10 g of sample powder was dispersed in the solution constituted by water (90 mL) and triethanolamine (10 mL). A 300 W simulated solar xenon arc lamp was used as the light source and positioned above the photocatalytic reactor. Prior to photoirradiation, suspensions were dispersed by sonication for 5 min and then, the reactive system was evacuated for 20 min to ensure air completely removed. The reaction was performed at 5 °C. The generated hydrogen gas was sampled and measured using online gas chromatography (Agilent, GC-6820) and thermal conductivity detector (TCD, Ar carrier).

The apparent quantum efficiency (AQE) was measured using a Pyrex top-irradiation-type reaction vessel with an ultraviolet lamp (λ= 254 nm and 302 nm). The apparent quantum yield (AQY) of the NBTO SCNs was calculated basing on the following equation:

$$AQY\,(\%) = \frac{2 \times H_2\ molecules\ producted}{Number\ of\ incident\ photos} \times 100$$

The photocatalytic properties of the as-obtained sample were investigated by the photodegradation of Rhodamine B (RhB) dye and tetracycline. Typically, 0.10 g of NBTO SCNs was dispersed in 100 mL of RhB or tetracycline solution (c = 10 mg L^{-1}) in a quartz reactor. Prior to photoirradiation, the suspensions were sonicated for 5 min and continuously stirred in the dark for 40 min, in order to achieve the adsorption-desorption equilibrium between catalyst particles and pollutants. At varied irradiation time intervals, three milliliter suspensions were taken from the reaction system and immediately centrifuged at 10000 rpm for 5 min, in order to completely remove the catalyst particles. The residual pollutants concentration in the supernatant was determined by UV-vis spectrophotometer (HITACHI, UH-5300).

Photoelectrochemical measurements

The Mott-Schottky was carried out using electrochemical workstation (CHI604C) with a standard three-electrode cell system. The photocatalyst sample was deposited on a fluorine-doped tin oxide (2 cm × 2 cm) plate as the working electrode, and then dried in oven at 120 °C for 10 h. Pt foil, Ag/AgCl and 0.5 M Na_2SO_4 solutions were used as counter, reference electrode and electrolyte, respectively.

Computational details

Density functional theory (DFT) calculations were performed to investigate the electronic band structures of $Na_{0.5}Bi_{2.5}Ta_2O_9$, $NaTaO_3$, and $BiTaO_4$ using the generalized gradient approximation (GGA-PBE). The density of states (DOS) plots of three samples obtained from the first principles DFT calculations. CASTEP package based on the plane-wave-pseudo potential approach was used to perform DFT calculations.

Results and discussion

Figure S1a shows the X-ray photoelectron spectroscopy (XPS) spectrum of the NBTO SCNs within Ta 4f, Bi 4f, Ta 4d, C 1s, Ta 4p, Bi 4d, O 1s, Bi 4p and Na 1s peaks. Two peaks of O 1s (Figure S1b), centered at around 530.1 eV and 531.4 eV, in which the higher peak was assigned to lattice oxygen while the lower shoulder one was assigned to oxygen vacancies.[3] The Ta $4f_{7/2}$ and $4f_{5/2}$ peaks were observed at 25.8 eV and 27.5 eV, respectively (Figure S1c), which confirmed that the Ta element existed mainly in the form of Ta^{5+}. The Na 2p peak at 29.0 eV was attributed to Na^+.

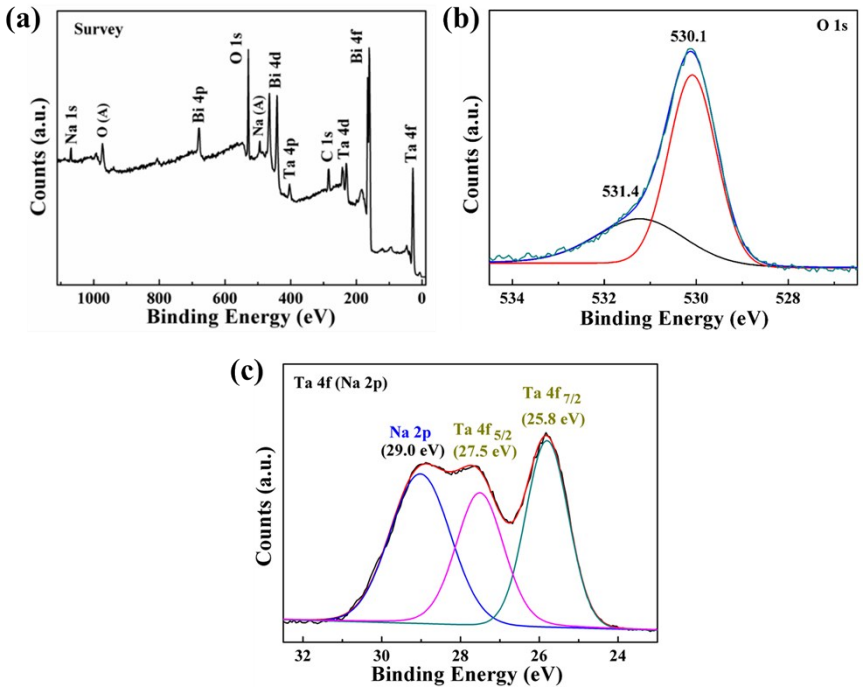

Figure S1. (a) Survey XPS spectrum, High-resolution XPS spectra of (b) O 1s, and (c) Ta 4f and Na 2p for the NBTO SCNs.

Table S1 Theoretical and observed atom ratio of NBTO SCNs

	Na	Bi	Ta
Theoretical atom ratio	0.5	2.5	2
Observed mass concentration (mg/L)	0.022	0.973	0.682
Observed atom ratio	0.52	2.47	2

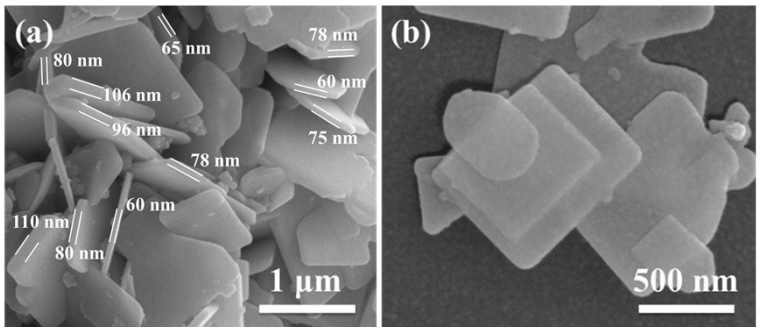

Figure S2. SEM images of NBTO SCNs under different magnification.

As shown in Figure S3,

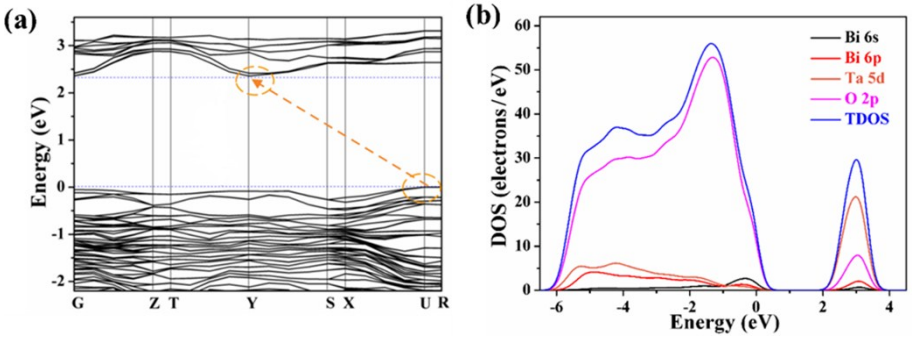

Figure S3. Band structure (a) and corresponding electronic DOS plot (b) of NBTO SCNs: total density of state (TDOS) plot and ion-decomposed (Bi 6s, Bi 6p, Ta 5d and O 2p) plots.

The morphology of the prepared samples was characterized by SEM. As shown in Figure S4a, the as-prepared $NaTaO_3$ particles present an approximately square structure with a smooth surface. These particles exhibit a wide size distribution in the range of 0.3 to 1.5 μm. The BET specific surface area of $NaTaO_3$ is 1.47 $m^2\ g^{-1}$. The $BiTaO_4$ presents irregular large bulk particle (Figure S4b), and the BET specific surface area of $BiTaO_4$ is 0.66 $m^2\ g^{-1}$. As shown in Figure S2, SEM images reveal that the NBTO SCNs is composed of large-scale plate-like structures with widths of 0.4−1 μm and thicknesses of 60−110 nm. The BET specific surface area of NBTO SCNs is 4.512 $m^2\ g^{-1}$.

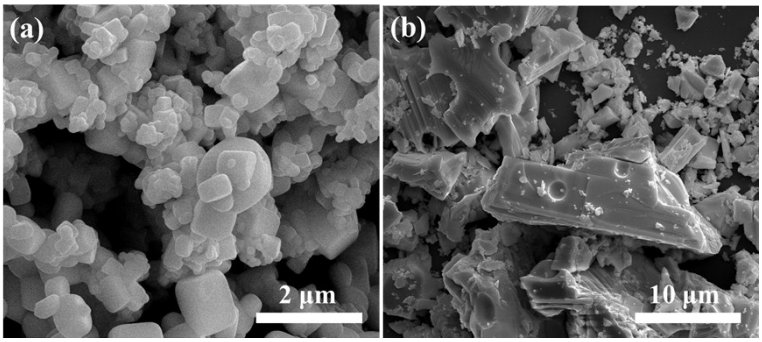

Figure S4. SEM images of (a) $NaTaO_3$ and (B) $BiTaO_4$.

The photocatalytic performances of $NaTaO_3$, $BiTaO_4$ and NBTO SCNs were evaluated by decomposition of RhB solution. As shown in Figure S5a and Figure S5c, the RhB dye can be completely degraded after 25 min in the presence of photocatalyst NBTO SCNs under simulated sunlight irradiation, while the $NaTaO_3$ and $BiTaO_4$ show negligible photodegradation activities. In addition, the photocatalytic activities of three photocatalysts were further appraised by the degradation of RhB dye under the visible light irradiation ($\lambda > 400$ nm). As shown in Figure S5b, the degradations of RhB over $NaTaO_3$ and $BiTaO_4$ were negligible, while the RhB solution exhibited excellent photocatalytic degradation rate in the presence of NBTO SCNs. These results imply that the NBTO SCNs exhibit strong dye sensitization effect when degrading the colored RhB due to the large bandgap (3.53 eV).

The photocatalytic performances of the $NaTaO_3$, $BiTaO_4$, and NBTO SCNs were also evaluated by decomposition of tetracycline solution. The results are shown in Figure S5d. The photolysis of tetracycline is negligible in presence of $NaTaO_3$ or $BiTaO_4$ as the photocatalyst, and the NBTO SCNs shows excellent photocatalytic activity for the tetracycline degradation reaction. The decomposition rate of tetracycline solutions in the presence of NBTO SCNs is 91.5% after 60 min. All of these results confirm that the as-synthesized NBTO SCNs can efficiently enhance the photocatalytic activity compared with $NaTaO_3$ and $BiTaO_4$.

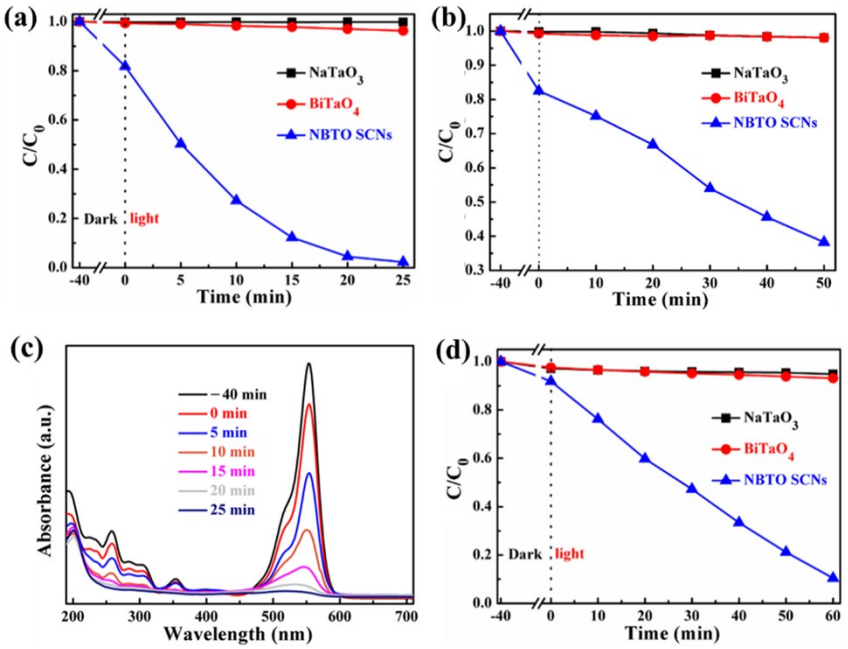

Figure S5. Time profiles of photocatalytic degradation of RhB over the $NaTaO_3$, $BiTaO_4$, and NBTO SCNs (a) under simulated sunlight irradiation, and (b) under visible light irradiation. (c) Absorbance variation curves of the RhB solutions over NBTO SCNs under simulated sunlight irradiation. (d) Time profiles of photocatalytic degradation of tetracycline over the $NaTaO_3$, $BiTaO_4$, and NBTO SCNs under simulated sunlight irradiation.

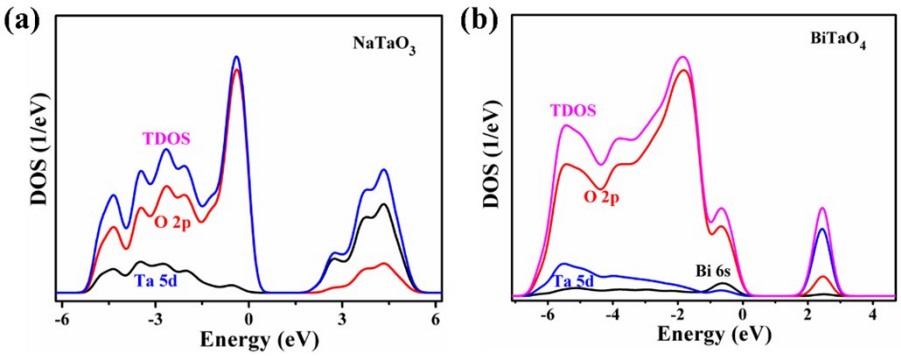

Figure S6. DOS plots for (a) $NaTaO_3$, and (b) $BiTaO_4$.

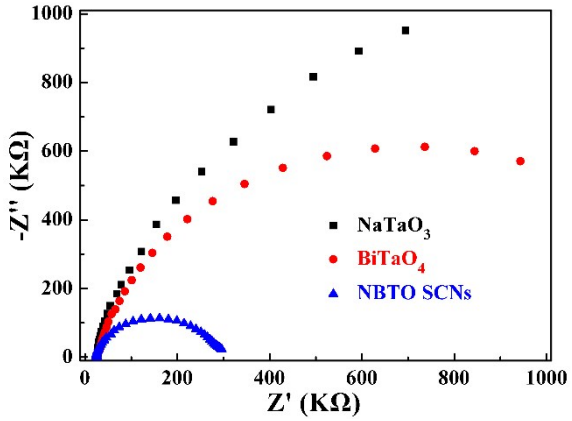

Figure S7. Electrochemical impedance spectroscopies (EIS) plots of $NaTaO_3$, $BiTaO_4$, and NBTO SCNs.

Table S2 Photocatalysts for water splitting to hydrogen

Photocatalyst	synthetic method	mass (g)	light source	aqueous	H_2 activity ($\mu mol \cdot h^{-1} \cdot g^{-1}$)	reference
TiO_2 amorphous	hydrolysis	1	450-W Hg	CH_3OH	6	4
$SrTiO_3$	Alfa-Ventron	0.5	450-W Hg	NaOH	NiO_x/~70	5
$BaTiO_3$	polymerized complex	0.1	300-W Xe (>420 nm)	CH_3OH	Pt/8	6
$Bi_4Ti_3O_{12}$	solid-state	1	450-W Hg	CH_3OH	Pt/0.6	7
$BiTaO_4$	solid-state	1	400-W Hg	pure water	4	8
NBTO SCNs	molten-salt	0.1	Simulated solar	triethanolamine	42	Present

References

1 H. Kato and A. Kudo, *J. Phys. Chem. B* 2001, **105**, 4285-4292.
2 R. S. Roth and J. L. Waring, *Am. Mineral.* 1963, **48**, 1348-1353.
3 J. Wang, Z. Wang, B. Huang, Y. Ma, Y. Liu, X. Qin, X. Zhang and Y. Dai, *ACS Appl. Mater. Interfaces* 2012, **4**, 4024−4030.

4 J. Jitputti, T. Rattanavoravipa, S. Chuangchote, S. Pavasupree, Y. Suzuki and S. Yoshikawa, *Catal. Commun.*, 2009, **10**, 378-382.
5 K. Domen, A. Kudo, T. Onishi, N. Kosugi and H. J. Kuroda, *Phys. Chem.* 1986, **90**, 292-295.
6 K. Maeda, *ACS Appl. Mater. Interfaces,* 2014, **6**, 2167−2173.
7 A. Kudo and S. Hijii, *Chem. Lett.*, 1999, **28**, 1103-1104.
8 Z. Zou, J. Ye, K. Sayama and H. Arakawa, *Chem. Phys. Lett.*, 2001, **343**, 303-308.